



**Suppression of exciton dephasing in sidewall-functionalized
carbon nanotubes embedded into metallo-dielectric
antennas**

Journal:	<i>Nanoscale</i>
Manuscript ID	NR-ART-05-2018-003542.R2
Article Type:	Paper
Date Submitted by the Author:	02-Jun-2018
Complete List of Authors:	Shayan, Kamran; Stevens Institute of Technology, Department of Physics He, Xiaowei; Los Alamos National Laboratory, MAP-CINT: center for integrated nanotechnology Luo, Yue; Stevens Institute of Technology, Department of Physics Rabut, Claire; Stevens Institute of Technology, Department of Physics Li, Xiangzhi; Stevens Institute of Technology, Department of Physics Hartmann, Nicolai; LMU Muenchen, Blackburn, Jeffrey; NREL, Doorn, Stephen; Los Aamos National Laboratory, Htoon, Han; Los Alamos National Lab, MPA-CINT Strauf, Stefan; Stevens Institute of Technology, Department of Physics

Suppression of exciton dephasing in sidewall-functionalized carbon nanotubes embedded into metallo-dielectric antennas

Kamran Shayan^a, Xiaowei He^b, Yue Luo^a, Claire Rabut^a, Xiangzhi Li^a, Nicolai F. Hartmann^b, Jeffrey L. Blackburn^c, Stephen K. Doorn^b, Han Htoon^b and Stefan Strauf^{a*}

^a *Department of Physics, Stevens Institute of Technology, Hoboken, NJ 07030, USA.*

E-mail: strauf@stevens.edu

^b *Center for Integrated Nanotechnologies, Materials Physics and Applications Division, Los Alamos National Laboratory, New Mexico, 87545, USA*

^c *National Renewable Energy Laboratory, Golden, Colorado 80401, USA.*

Covalent functionalization of single-walled carbon nanotubes (SWCNTs) is a promising route to enhance the quantum yield of exciton emission and can lead to single-photon emission at room temperatures. However, the spectral linewidth of the defect-related E_{11}^* emission remains rather broad. Here we systematically investigate the low-temperature exciton emission of individual SWCNTs that have been dispersed with sodium-deoxycholate (DOC) and polyfluorene (PFO-BPy), are grown by laser vaporization (LV) or by CoMoCat techniques and are functionalized with oxygen as well as 3,5-dichlorobenzene groups. The E_{11} excitons in oxygen-functionalized SWCNTs remain rather broad with up to 10 meV linewidth while exciton emission from 3,5-dichlorobenzene functionalized SWCNTs is found to be about one order of magnitude narrower. In all cases wrapping with PFO-BPy provides significantly better protection against pump induced dephasing as compared to DOC. To furthermore study the influence of exciton localization on pump-induced dephasing we have embedded the functionalized SWCNTs into metallo-dielectric antenna cavities to maximize light collection. We show that 0D excitons attributed to the E_{11}^* emission of 3,5-dichlorobenzene quantum defects of LV-grown SWCNTs can display near resolution-limited linewidths down to 35 μeV . Interestingly, these 0D excitons give rise to a 3-fold suppressed pump-induced exciton dephasing compared to the E_{11} excitons in the same SWCNT. These findings provide a foundation to build a unified description on emergence of novel optical behavior from the interplay of covalently introduced defects, dispersants, and exciton confinement in SWCNTs and might further lead to the realization of indistinguishable photons from carbon nanotubes.

Introduction

Single-walled carbon nanotubes (SWCNTs) are promising absorbers and emitters for optoelectronic devices, biological imaging, molecular sensing, and quantum photonic applications.^{1,2} The optical emission of SWCNTs from the E_{11} energy state is dominated by radiative recombination of excitons featuring large exciton binding energy up to 400 meV,³ that makes them particularly promising for room temperature applications. A severe drawback is that the optical quantum yields (QY) from E_{11} excitons remains rather low with typical values of 2-7%.⁴⁻⁶ These low QYs are detrimental for optoelectronic device applications since the predominance of nonradiative (NR) optical recombination leads to strongly reduced optical emission rates of nanoscale light sources. One possible way to overcome that issue is to enhance the radiative rate over the NR rate by utilizing the Purcell effect. By coupling the exciton emission of individual SWCNTs to high quality (Q) factor optical modes created in fiber-tip-based dielectric cavities QY=11% has been demonstrated,⁶ and by further reducing mode volume QY=40% was reached.⁷ This approach however requires moving external mirrors and works only in a narrow spectral band and is thus not easily scalable to address large numbers of SWCNTs with varying chirality or for on-chip geometries. In contrast, by coupling to plasmonic nanocavity arrays on-chip one can enhance QY over a broad spectral range covering various SWCNTs chiralities with best values up to QY=64% in our recent demonstration.⁸

Another promising approach is to directly alter the QY of the exciton emission in SWCNTs by utilizing covalent surface functionalization to trap excitons in energetically deep states, thereby avoiding coupling to the environment and possibly to NR recombination channels. By taking advantage of the unique morphology of SWCNTs, a wide variety of approaches to introduce defects and impurities into SWCNTs exists.⁹ For example, chemical functionalization with oxygen forms ether and epoxide groups leading to the creation of strongly localized exciton emission located about 100-300 meV (E_{11}^*) below the E_{11} state.¹⁰⁻¹² These oxygen-related localization centers can be created by depositing SiO_2 onto SWCNTs, which has also led to the first observation of photon antibunching at room temperature from the E_{11}^* exciton emission that approaches telecom wavelength.¹³⁻¹⁴ Other agents for covalent sidewall functionalization such as 4-chlorobenzenediazonium tetrafluoroborate have been shown to lead to photoluminescence (PL) quenching at high concentrations,¹⁵ while more recent work demonstrated that covalently attached aryl groups from aryl diazonium salts introduced at lower concentration levels can form sp^3 defects on the sp^2 lattice that lead to reported QY of the E_{11}^* transition of up to 28%,¹⁶ about an order of magnitude higher than the QY of E_{11} excitons. Previous work showed furthermore that the defect-related E_{11}^* emission is very sensitive to the SWCNT chirality leading to a systematic enhancement of the QY with decreasing nanotube diameter being most pronounced in the 800-1000 nm wavelength band that is covered by (5,4)-(7,5) chirality SWCNTs.¹⁶ A similar trend was recently observed in the temporal dynamics of the exciton emission showing that the narrowest SWCNTs of (5,4) chirality show the longest spontaneous emission times (T_1) up to 600 ps, while larger (7,5) SWCNTs can be as fast as 77 ps for the E_{11}^* excitons.¹⁷

Beyond these initial studies a better understanding of the relevant interplay between molecular functionalizing groups, dispersion agent, and degree of exciton localization is required to optimize the optical and transport properties of functionalized SWCNTs in applications such as light-harvesting photovoltaic devices and quantum light sources. Specifically, single-photon sources ideally require the emission of indistinguishable photons, i.e. long photon coherence times (T_2) that are equivalent to ultra-narrow spectral linewidth corresponding to the condition $T_2 \sim 2T_1$.¹⁸ So far, the reported E_{11}^* emission in oxygen-

functionalized SWCNTs are found to be rather broad, covering several meV even at cryogenic temperatures¹³ and emitted photons are thus orders of magnitude away from being indistinguishable. As is well-known for the E_{11} exciton emission, the spectral PL linewidth is affected by pronounced exciton-phonon dephasing^{8,18} as well as by detrimental pump-induced spectral diffusion due to surfactant or substrate interactions.¹⁹⁻²¹ It was recently shown that the interaction of E_{11} excitons with acoustic phonons can be effectively suppressed in polyfluorene (PFO-BPy) wrapped SWCNTs, leading to record-narrow spectral linewidth down to 18 μeV implying transform limited photons.⁸ However, values for the E_{11}^* excitons in 3,5-dichlorobenzene functionalized SWCNTs are still significantly broader, with 270 μeV linewidth.²²

Here we systematically investigate the low-temperature exciton emission (E_{11} and E_{11}^*) of individual SWCNTs that have been dispersed with sodium-cholate (DOC) and PFO-BPy, are grown by laser vaporization (LV) as well as the CoMoCat technique and are functionalized with either oxygen or 3,5-dichlorobenzene functional groups. We show that the narrowest E_{11}^* linewidths (35 μeV) are achieved with SWCNTs grown by LV-grown, wrapped with PFO-BPy and functionalized with 3,5-dichlorobenzene. Remarkably, we also find that the pump power induced broadening for E_{11}^* excitons is suppressed by 3-fold when compared to the E_{11} excitons in the same SWCNT, indicating that deeper confinement leads to better exciton protection from pump-induced dephasing.

Results and Discussion

To study the influence of the dispersant as well as the functional groups we will first focus on the spectral linewidth of the E_{11} exciton transition targeting particularly individual SWCNTs with (5, 4) and (6, 4) chiralities. As illustrated in **Fig. 1a**, under 1.589 eV (780 nm) laser excitation, excitons are pumped non-resonantly below the E_{22} exciton state, where absorption occurs via phonon-sideband transitions.^{8, 23} The corresponding emission spectra are shown in **Fig. 1b**, with signatures of the E_{11} exciton zero-phonon line (ZPL) at 1.44 eV (860 nm) for (5,4) SWCNTs (top panel) and at 1.39 eV (890 nm) for the (6,4) SWCNTs (bottom panel). The Raman G-mode (D-mode) is visible in all optical spectra at 1.385 eV (1.425 eV). While pristine SWCNTs are dominated by the E_{11} exciton emission and do not show any pronounced peaks in the long wavelength regime around 1000 nm, in contrast the spectra of all 3,5-dichlorobenzene-functionalized SWCNTs are dominated by the characteristic E_{11}^* exciton emission around 1000-1025 nm (1.20-1.24 eV). Note that the spectra in the E_{11} regime are magnified by six-fold to produce comparable signal. In addition, the silicon detector quantum efficiency is more than five-fold lower at 1020 nm (8%) as compared to 890 nm (45%), resulting in a relative zero-phonon line (ZPL) intensity ratio E_{11}^*/E_{11} of 34. This strong suppression of the E_{11} exciton transition on the sidewall-functionalized SWCNTs clearly indicates that optically pumped excitons relax quickly into the lower lying E_{11}^* defect states before radiative recombination can occur through the E_{11} channel. This is consistent with the picture that has been developed that defect state population occurs by diffusive trapping of the band-edge E_{11} exciton^{17,24}. **Fig. 1c** demonstrates emission from 10 individual SWCNTs that are dominated by one spectrally-sharp E_{11}^* exciton emission peak, accompanied in some cases by 1-2 additional emission lines with significantly weaker intensity. We have recently shown that the aryl defect sites in 3,5-dichlorobenzene-functionalized SWCNT can give rise to an exciton manifold with 6 spectrally distinct transitions that occur over a wide wavelength range of 300 nm resulting from topological variations in the chemical binding configuration of the monovalent aryl

groups²². The highest lying energy defect state is the Ortho_{L90} configuration²² that we attribute here to the origin of the E_{11}^* emission. While lower lying states in other configurations might be present, they are naturally excluded in our study since they are not spectrally observable with the silicon detector in our study.

Fig. 2a illustrates the effect of pump-induced broadening of the ZPL for the case of the E_{11} exciton emission of an LV-grown SWCNT dispersed with PFO-BPy. Spectra recorded at lowest pump powers display only a single ZPL transition while at higher pump powers (0.6-4 mV) additional energetically broad shoulders appear on the low-energy side. We have recently shown that side peaks can originate from phonon confinement effects and are particularly pronounced at elevated pump power or temperature.^{18, 22, 25} Here we focus our study on the ZPL lineshape and carried out simple Lorentzian lineshape fits that ignore the additional phonon wings. The extracted Lorentzian linewidth values of the ZPL are plotted in **Fig. 2b-c** as a function of pump power comparing two surfactants (DOC and PFO) as well as two functional groups (oxygen and 3,5-dichlorobenzene). Exemplary pump power traces are shown in each case for two different SWCNTs. Most striking is that oxygen doping leads to significantly broader ZPL as compared to aryl sidewall functionalization, particularly at highest pump powers. For the case of oxygen doping and DOC dispersant the ZPL remains broad with 5-10 meV linewidth even at lowest pump powers (**Fig. 2b**, top). In contrast, PFO-BPy-wrapped SWCNTs appear to be significantly better protected from pump-induced exciton dephasing and pump-induced spectral diffusion effects, displaying sub-meV linewidth at low pump power, which is in line with previous reports on pristine SWCNTs.^{8, 18, 25}

However, under strong pumping oxygen-functionalized SWCNTs reach back to 5 meV linewidth even when protected by PFO-BPy, indicating that the doping procedure induces a significant amount of mobile charges in the exciton vicinity that can give rise to pump-induced spectral diffusion broadening. This is consistent with density functional theory modelling and the contrasting blinking behavior observed for oxygen vs. aryl functionalization.²⁴ In contrast to the case of oxygen, the SWCNTs functionalized with 3,5-dichlorobenzene always display narrow linewidth values that are largely independent of the dispersant and remain spectrally narrow even under the highest pump powers, with values of 0.3-0.8 meV (**Fig. 2c**).

The growth technique of the SWCNT host crystal plays an additional role in the achievable exciton linewidth. To this end we compare in **Fig. 3** SWCNTs that are commercially available as CoMoCat SWCNT, with those that have been grown via laser-vaporization (LV). For this comparison, both sets of SWCNTs were dispersed with PFO-BPy and underwent the same sidewall functionalization procedure with 3,5-dichlorobenzene (see methods). The result is a striking difference in ZPL linewidth of the E_{11}^* exciton emission, showing that CoMoCat SWCNTs typically do not reach into the sub-meV regime at low pump powers and remain about 5-6 times broader as compared to the LV-grown SWCNTs. We note that while this comparison was carried out for slightly different sonication conditions no straightforward evidence is known that this would cause a six-fold variation in exciton linewidth. There is rather more evidence that the difference is caused by the growth technique since our findings are similar to reports for the E_{11} emission in pristine SWCNTs with high crystalline quality for LV growth.²⁶ Apparently, if the goal is to realize spectrally narrow exciton emission with near intrinsic properties the best combination is to utilize LV growth, PFO-BPy wrapping, and 3,5-dichlorobenzene functionalization.

With SWCNTs samples prepared in this way we now turn to a systematic study that compares the E_{11} exciton with the E_{11}^* exciton linewidth in the same SWCNT. The key

question is if the strong localization of the exciton in the vicinity around the 3,5-dichlorobenzene group leads to significantly better protection of E_{11}^* against environmental dephasing as compared to the energetically shallower disorder localization of the E_{11} exciton.¹³ To answer this question more systematically, and to enable the recording of optical spectra at lowest excitation powers, we have embedded the functionalized SWCNT into metallo-dielectric antenna (MDA) arrays. As we have shown recently for the case of pristine SWCNTs, light collection efficiencies (LCE) up to 92% for the E_{11} emission at 890 nm can be achieved by coupling the exciton emission to an MDA.²⁵ Following the three-layer design rule $n_1 < n_2 < n_3$ introduced by Lee et al.²⁷, we have assembled here arrays of MDA's with embedded functionalized SWCNTs as shown schematically in **Fig. 4a-b**. The patterned air gaps ($n_1=1$) on top of a metal mirror (Ag) are created by capping with a polystyrene (PS) layer ($n_2=1.56$) utilizing a polymer-release-transfer technique that is similar to the assembly of monolayer heterostructures.²⁸ With the PS layer in place, which also protects the air gaps from filling with solvents, SWCNTs were drop casted and subsequently functionalized (see methods), followed by a second layer of PS and capping with a 300 μm commercial sapphire substrate ($n_3=1.76$). **Fig. 4c** shows an optical image of the fully assembled MDA stack featuring an array of square-shaped MDA cavities with 3 μm side length. Note, while the use of a 300 μm thick sapphire substrate will substantially broaden the far-field emission profiles (**Fig. 4d**), the achievable LCE when collected with a high numerical aperture (NA = 0.81, collection angle $\pm 54^\circ$) microscope objective degrades only slightly at 1000 nm from 85% for 200 nm sapphire thickness to 80% at 300 μm thickness (**Fig. 4e**). As a result, embedding SWCNTs into the MDA allows for six-fold enhanced LCE as compared to a bare dipole emitter on a substrate (14%, dashed line in **Fig. 4e**).

An exemplary emission spectrum recorded at a pump power of 361 μW for E_{11}^* exciton transition of an LV-grown, PFO-BPy wrapped, and 3,5-dichlorobenzene functionalized SWCNT located inside the MDA cavity is shown in **Fig. 5a** together with a single Lorentzian fit that yields a linewidth of 172 μeV . Lorentzian exciton linewidth values of the ZPL are shown in **Fig. 5b** as a function of excitation power. Initially the linewidth increases sublinearly until saturation sets in at higher pump powers (**Fig. 5b**). The narrowest linewidth for the doping-induced E_{11}^* approaches at lowest pump power the resolution limit and is found from Voigt deconvolution to be 35 μeV , which is significantly narrower as compared to previously observed linewidth values of about 270 μeV in 3,5-dichlorobenzene functionalized SWCNT.²² This is a combined result of the six-fold enhanced LCE provided by the MDA that allows recording exciton spectra down to lower pump power limits as well as the use of LV-grown material (**Fig. 3**), as compared to CoMoCat material in Ref. 22.

Given that the ZPL stays well-defined with sub-1-meV values even at highest pump powers one can exclude temperature-induced linewidth broadening effects by the incident laser power. A significantly increased SWCNT temperature would lead to thermal break-up of the fragile phonon confinement, with their characteristic confinement energy of about 2 meV, that gives rise to drastic linewidth broadening up to 10 meV at temperatures above about 80 K or under laser-induced plasmonic heating.⁸ Likewise, we exclude exciton-exciton scattering as a cause of linewidth broadening that is often observed in 1D excitons,²⁹ since the observation of strong photon antibunching in our previous work^{8,13,14} indicates that the number of excitons in these localized systems at cryogenic temperatures is well below 2. In contrast, the fact that the exciton ZPL remains Lorentzian even up to highest pump powers (**Fig.5a**) implies a homogenous dephasing process, such as random telegraph noise caused by fluctuating charges in the exciton vicinity, as it is known for excitons in quantum dots.^{30,31} In this model one assumes that the laser pumps charges out of trap states with a concentration N that reside

in the vicinity of the exciton and cause rapid quantum-confined Stark-shifts onto the Lorentzian exciton spectrum, i.e. a linewidth broadening in time-integrated spectra. Based on Monte-Carlo simulations of the trapping and detrapping of single charges, it is predicted that the additional linewidth broadening Γ_{SD} due to pump-induced charge fluctuations follows as $\Gamma_{SD} \sim \sqrt{N}$. Since N is linearly proportional to pump power P it follows that $\Gamma_{SD} \sim \sqrt{P}$, i.e. the pump-induced linewidth broadening follows a slope exponent of 0.5.^{30,31} The black solid-line in **Fig.5b** plots the total linewidth $\Gamma = \Gamma_0 + \Gamma_{SD} = \Gamma_0 + \alpha\sqrt{P}$ for one case, where the constant Γ_0 is the residual linewidth (35 μeV) and α a fit parameter, providing striking agreement between experimental linewidth data and theoretical predictions of the charge-trap model. The linewidth slope is also in agreement with comparable results for the E_{11} exciton of pristine SWCNTs in our previous work.⁸

It is furthermore expected that the degree of linewidth broadening should depend on the degree of 0D exciton localization, i.e. excitons localized into energetically deeper states are better screened from pump-induced charge fluctuations. To this end we point out that our functionalized SWCNTs display emission from both E_{11} excitons localized by random (energetically shallow) potential fluctuations with single-photon antibunching typically vanishing above 100 K, as well as emission from the energetically deeper ($\Delta E \sim 200$ meV) localized E_{11}^* excitons bound to the location of the 3,5-dichlorobenzene that displays antibunching up to room temperature. This allows a clear comparison of linewidth values for 0D excitons with strongly varying confinement energy within the same SWCNT. The top panel in **Fig. 5b** shows the resulting ZPL linewidth ratio between E_{11} and E_{11}^* , which indicates that at each pump power the resulting linewidth of the defect-localized exciton is three-fold narrower as compared to E_{11} excitons. This signature clearly indicates reduced environment interaction and susceptibility to pump-induced dephasing for the deeper localized exciton states.

In the trap-state model the three-fold reduced exciton linewidth corresponds to an effective reduction of the charge trap concentration N by a factor of 9 ($N \sim \Gamma^2$) that is interacting with the E_{11}^* excitons as compared to the E_{11} . While the exact energy structure of these trap states is unknown, it is plausible to assume that E_{11}^* excitons are effectively more detuned from the trap states and thus are less affected by the pump-induced Stark-shifts. At the microscopic level the concept of exciton emission oscillator strength f provides additional insights. It is known from time-dependent density functional theory calculations that f for aryl-functionalized SWCNT excitons is systematically smaller than f for pristine SWCNT excitons. For example, the ortho L_{90} configuration of the sidewall-attached aryl amounts to $f=9$, while in contrast the pristine E_{11} exciton has an oscillator strength of $f=34$, or approximately $f=3-4$ per nm length of carbon nanotube.³² For the case of cryogenic spectroscopy of pristine SWCNTs typical E_{11} localization in random potential fluctuations are reported on length scales of 3-5 nm^{18,33,34,35}, resulting in a range for the exciton oscillator strength of $f=9-20$. The systematically larger oscillator strength of E_{11} excitons leads directly to a stronger Stark-interaction between the exciton dipole and the electric fields of the charge fluctuations, and thus a broader ZPL. While a detailed theoretical model is beyond the scope of this work, our experimental findings provide a clear path to create quantum light emission from functionalized SWCNTs with superior spectral linewidth.

Experimental

Carbon nanotube synthesis

CoMoCat SG65i SWCNTs were purchased from Southwest Nanotechnologies. Samples are produced by the CoMoCATTM synthesis process and the commercial supplier reports an average diameter of 0.78 nm and content of (6,5) chirality that is larger than 40%. The laser vaporization (LV) grown SWCNTs for this study were produced in the LV process³⁶ at a furnace temperature of 800 °C, and all syntheses were run at a power density of ~ 100 W/cm² ($\lambda = 1064$ nm, Nd:YAG). Such samples contain a broad distribution of small-diameter SWCNTs ($0.6 < d < 1.2$ nm), with significant amounts of (5, 4) and (6, 4) nanotubes.

Carbon nanotube dispersion

Surfactant dispersion: LV-grown SWCNTs were dispersed in a 1.04% (m/v) sodium deoxycholate (DOC) solution in nanopure H₂O at a nanotube concentration of 1mg/mL, base sonication for 1 hour with a tip sonicator of 1/4" at a power output of 0.9 W/mL (Sonic Vibra Cell with tip CV18-9909, 8W) while immersed in an ice bath. (6,5) chirality nanotubes were then sorted out by the aqueous two-phase extraction method³⁷.

Polymer dispersion: For the case of CoMoCat material (data in Figure 3) 20 mg of PFO-bpy was dissolved in 10 mL of toluene, after which 10 mg of CoMoCAT SG65i SWCNTs was placed into the poly[(9,9-dioctylfluorenyl-2,7-diyl)-alt-co-(6,60-{2,20-bipyridine})] (PFO-bpy) solution. These mixtures were bath-sonicated for 1 hour with no cooling, after which the samples were immediately centrifuged at 30 000g (Beckman ultracentrifuge using a SW32Ti rotor) in thin polyallomer centrifuge tubes for 5 min at 20°C. For the case of LV-grown material 1 mg/mL of raw LV soot was mixed into a solution of 2 mg/mL of PFO-BPy in toluene. This solution was then sonicated with a 1/2 in. probe tip for 30 min at 40% power (Cole-Parmer CPX 750) in a bath of cool (18°C) flowing water for heat dissipation. After sonication, solutions were centrifuged at 30 000g for 5 min (Beckman ultracentrifuge using a SW32-Ti rotor). For cavity-integration PFO-BPy dispersed LV-grown SWCNTs in toluene were deposited directly onto the MDA arrays followed by 105 °C baking on a hot plate for 3 hours.

Surface functionalization

Surface functionalization was carried out in a dip-doping process. To this end the substrate containing dried out LV-grown SWCNTs, either with DOC or PFO-BPy wrapping as a dispersant, have been immersed into the aqueous solution of 3,5-dichlorobenzene diazonium (0.7 mg/mL in nano-pure water) or, alternatively, exposed to a droplet of the same solution for 3-5 minutes. The doping process is stopped by putting the substrate into 1% (w/v) DOC for another 3 minutes. The substrate containing functionalized SWCNTs are then dried in air before optical measurements. To prevent substrate-induced spectral diffusion, we have coated the Si/SiO₂ carrier substrates with a 2 nm thin layer of Al₂O₃ following our previous work.⁸ In addition, we have also carried out oxygen doping using LV-grown SWCNTs by over-coating with a 10 nm electron-beam-deposited SiO₂ layer. The deposition rate was 0.2 nm s⁻¹ using 99.99% pure SiO₂ target (CERAC). The base pressure of the chamber was 2.8×10^{-8} torr and the substrate was maintained at room temperature.

Photoluminescence spectroscopy

Micro-photoluminescence (μ -PL) measurements were taken inside a closed-cycle cryostat with a 3.8 K base temperature and ultralow vibration (attodry1100) at a pressure of 10^{-6} bar. A red laser diode, emitting at 780 nm in continuous wave mode was used for excitation. A laser

spot size of about 0.85 micron was achieved using a cryogenic microscope objective with numerical aperture of 0.82. The relative position between sample and laser spot was adjusted with cryogenic piezo-electric xyz-positioners. Spectral emission from the sample was collected in a multimode fiber, dispersed using a 0.75 m focal length spectrometer, and imaged by a liquid nitrogen cooled silicon CCD camera.

Conclusions

We have shown that the E_{11} excitons in oxygen-functionalized SWCNTs remain rather broad with up to 10 meV linewidth at high pump powers (5 mW) while, in contrast, the spectral linewidth in 3,5-dichlorobenzene functionalized SWCNTs is found to be about one order of magnitude narrower. In all cases, wrapping with PFO-BPy provides significantly better protection against pump induced dephasing as compared to DOC. To study the influence of exciton localization on pump-induced dephasing we have further embedded the functionalized SWCNTs into an MDA cavity to enhance light extraction. Our data set demonstrates that the strong localization of 0D excitons attributed to the E_{11}^* emission of 3,5-dichlorobenzene quantum defects are significantly better at protecting against environmental dephasing, leading to a 3-fold suppression of pump-induced broadening compared to the E_{11} excitons in the same SWCNT. Even at highest pump powers the E_{11}^* emission can be as narrow as 110 μeV (~ 175 μeV on average), which is promising towards efficient single-photon sources that maintain their coherent properties despite significant charge fluctuations in the device.

Conflicts of interest

There are no conflicts to declare.

Acknowledgements

We like to thank Sergei Tretiak for discussions. S.S. acknowledges financial support by the National Science Foundation (NSF) under award DMR-1506711 and NSF award ECCS-MRI-1531237. J.B. gratefully acknowledges funding from the Solar Photochemistry Program of the U.S. Department of Energy, Office of Science, Basic Energy Sciences, Division of Chemical Sciences, Geosciences and Biosciences, under Contract No. DE-AC36-08GO28308 to NREL. This work was performed in part at the Center for Integrated Nanotechnologies, a U.S. Department of Energy, Office of Science User Facility. This work was funded in part by LANL LDRD support.

References

1. R. Ihly, K.S. Mistry, A.J. Ferguson, T.T. Clikeman, B.W. Larson, O. Reid, O.V. Boltalina, S.H. Strauss, G. Rumbles, J.L. Blackburn, *Nat. Chem*, 2016, **8**, 603-609.
2. S. Diao, J.L. Blackburn, G. Hong, A.L. Antaris, J. Chang, J.Z. Wu, B. Zhang, K. Cheng, C.J. Kuo, H. Dai, *Angew. Chem*, 2015, **127**, 14971-14975.
3. F. Wang, G. Dukovic, L.E. Brus, T.F. Heinz, *Phys. Rev. Lett*, 2004, **92**, 177401.
4. A. Nish, J.Y. Hwang, J. Doig, R.J. Nicholas, *Nat. Nanotechnol.* 2007, **2**, 640–646.
5. J. Lefebvre, D.G. Austing, J. Bond, P. Finnie, *Nano Lett*, 2006, **6**, 1603–1608.
6. A. Jeantet, Y. Chassagneux, C. Raynaud, P. Roussignol, J.S. Lauret, B. Besga, J. Estève, J. Reichel, C. Voisin, *Phys. Rev. Lett*, 2016, **116**, 247402.
7. A. Jeantet, Y. Chassagneux, T. Claude, P. Roussignol, J.S. Lauret, J. Reichel, J., C. Voisin, *Nano Lett.* 2017, **17**, 4184-4188.
8. Y. Luo, E.D. Ahmadi, K. Shayan, Y. Ma, K.S. Mistry, C. Zhang, J., Hone, J.L. Blackburn, S. Strauf, *Nat. Commun*, 2017, **8**, 1413.
9. S. Kilina, J. Ramirez, S. Tretiak, *Nano letters*, 2012, **12**, 2306-2312.
10. S. Ghosh, S.M. Bachilo, R.A. Simonette, K.M. Beckingham, R.B. Weisman, *Science*, 2010, **330**, 1656-1659.
11. Y. Miyauchi, M. Iwamura, S. Mouri, T. Kawazoe, M. Ohtsu, K. Matsuda, *Nat. Photonics*, 2013, **7**, 715-719.
12. X. Ma, L. Adamska, H. Yamaguchi, S.E. Yalcin, S. Tretiak, S.K. Doorn, H. Htoon, *ACS nano*, 2014, **8**, 10782-10789.
13. X. Ma, N.F. Hartmann, J.K. Baldwin, S.K. Doorn, H. Htoon, *Nat. Nanotechnol.*, 2015, **10**, 671-675.
14. X. He, N.F. Hartmann, X. Ma, Y. Kim, R. Ihly, J.L. Blackburn, W. Gao, J. Kono, Y. Yomogida, A. Hirano, T. Tanaka, *Nat. Photonics*, 2017, **11**, 577-582.
15. L. Cognet, D.A. Tsyboulski, J.D.R. Rocha, C.D. Doyle, J.M. Tour, R.B. Weisman, *Science*, 2007, **316**, 1465-1468.
16. Y. Piao, B. Meany, L.R. Powell, N. Valley, H. Kwon, G.C. Schatz, Y. Wang, *Nat chem*, 2013, **5**, 840-845.
17. N.F. Hartmann, K.A. Velizhanin, E.H. Haroz, M.Kim, X. Ma, Y. Wang, H. Htoon, S.K. Doorn, *ACS nano*, 2016, **10**, 8355-8365.
18. I. Sarpkaya, E.D. Ahmadi, G.D. Shepard, K.S. Mistry, J.L. Blackburn, S. Strauf, *ACS Nano*, 2015, **9**, 6383-6393.
19. W. Walden-Newman, I. Sarpkaya, S. Strauf, *Nano Lett.*, 2012, **12**, 1934-1941.
20. N. Ai, W. Walden-Newman, Q. Song, S. Kalliakos, S. Strauf, *ACS nano*, 2011, **5**, 2664-2670.
21. I. Sarpkaya, Z. Zhang, W. Walden-Newman, X. Wang, J. Hone, C.W. Wong, S. Strauf, *Nat. Commun.* 2013, **4**, 2152.
22. X. He, B.J. Gifford, N.F. Hartmann, R. Ihly, X. Ma, S.V. Kilina, Y. Luo, K. Shayan, S. Strauf, J.L. Blackburn, S. Tretiak, S.K. Doorn, H. Htoon, *ACS nano.*, 2017, **11**, 10785–10796.
23. J.L. Blackburn, J.M. Holt, V.M. Irurzun, D.E. Resasco, G. Rumbles, *Nano Lett*, 2012, **12**, 1398–1403.
24. N.F. Hartmann, S.E. Yalcin, L. Adamska, E.H. Hároz, X. Ma, S. Tretiak, H. Htoon, S.K. Doorn, *Nanoscale*, 2015, **7**, 20521-20530.
25. K. Shayan, C. Rabut, X. Kong, X. Li, Y. Luo, K.S. Mistry, J.L. Blackburn, S. Lee, S. Strauf, *ACS Photonics*, 2018, **5**, 289–294.

26. V. Ardizzone, Y. Chassagneux, F. Vialla, G. Delport, C. Delcamp, N. Belabas, E. Deleporte, P. Roussignol, I. Robert-Philip, C. Voisin, J.S. Lauret, *Phys. Rev. B*, 2015, **91**, 121410.
27. K. G. Lee, X. W. Chen, H. Eghlidi, P. Kukura, R. Lettow, A. Renn, V. Sandoghdar, S. Götzinger, *Nat. Photonics*, 2011, **5**, 166–169.
28. G. D. Shepard, J. V. Ardelean, O. A. Ajayi, D. Rhodes, X. Zhu, J.C. Hone, S. Strauf, *ACS nano*, 2017, **11**, 11550-11558.
29. D.T. Nguyen, C. Voisin, P. Roussignol, C. Roquelet, J.S. Lauret, G. Cassaboïs, *Phys. Rev. Lett.*, 2011, **107**, 127401.
30. A. Berthelot, I. Favero, G. Cassaboïs, C. Voisin, C. Delalande, P. Roussignol, R. Ferreira, J.M. Gérard, *Nat. Phys.*, 2006, **2**, 759.
31. M. Holmes, S. Kako, K. Choi, M. Arita, and Y. Arakawa, *Phys. Rev. B*, **92**, 115447
32. B.J. Gifford, S. Kilina, H. Htoon, S.K. Doorn, S. Tretiak, *J. Phys. Chem. C*, 2018, **122**, 1828–1838
33. F. Vialla, Y. Chassagneux, R. Ferreira, C. Roquelet, C. Diederichs, G. Cassaboïs, P. Roussignol, J. S. Lauret, C. Voisin, *Phys. Rev. Lett.*, 2014, **113**, 057402
34. G. Soavi, F. Scotognella, D. Viola, T. Hefner, T. Hertel, G. Cerullo, G. Lanzani, *Sci. Rep.*, 2015, **5**, 9681
35. C.D. Spataru, S. Ismail-Beigi, L.X. Benedict, S.G. Louie, *Phys. Rev. Lett.*, 2004 **92**, 077402.
36. K.S. Mistry, B.A. Larsen, J.L. Blackburn, *ACS Nano*, 2013, **7**, 2231–2239.
37. N. K. Subbaiyan, S. Cambré, A. N. G. Parra-Vasquez, E. H. Hároz, S. K. Doorn, J. G. Duque, *ACS Nano*, 2014, **8**, 1619–1628.

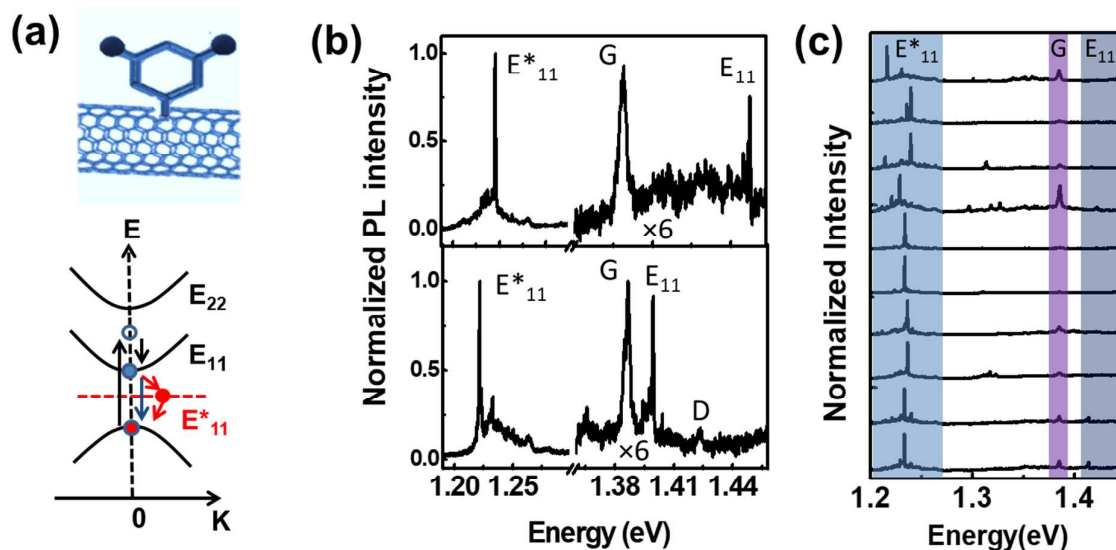


Fig.1 Low-temperature PL characterization of individual SWCNTs. (a) Schematic representation SWCNT with a 3,5-dichlorobenzene aryl group attached to the sidewall shown enlarged for clarity (upper panel). Schematic level scheme for quasi-resonant pumping of excitons into their excited states via one-phonon absorption processes involving the zone-center optical phonons (lower panel). (b) Low temperature PL spectra of 3,5-dichlorobenzene-functionalized LV-grown SWCNTs wrapped in PFO-BPy with (5, 4) chirality (upper panel) and (6, 4) chirality (lower panel). G and D: Raman signature of G-mode and D-mode phonons. (c) Overview of PL spectra from 10 individual 3,5-dichlorobenzene-functionalized (5,4) and (6,4) LV-grown SWCNTs wrapped in PFO-BPy.

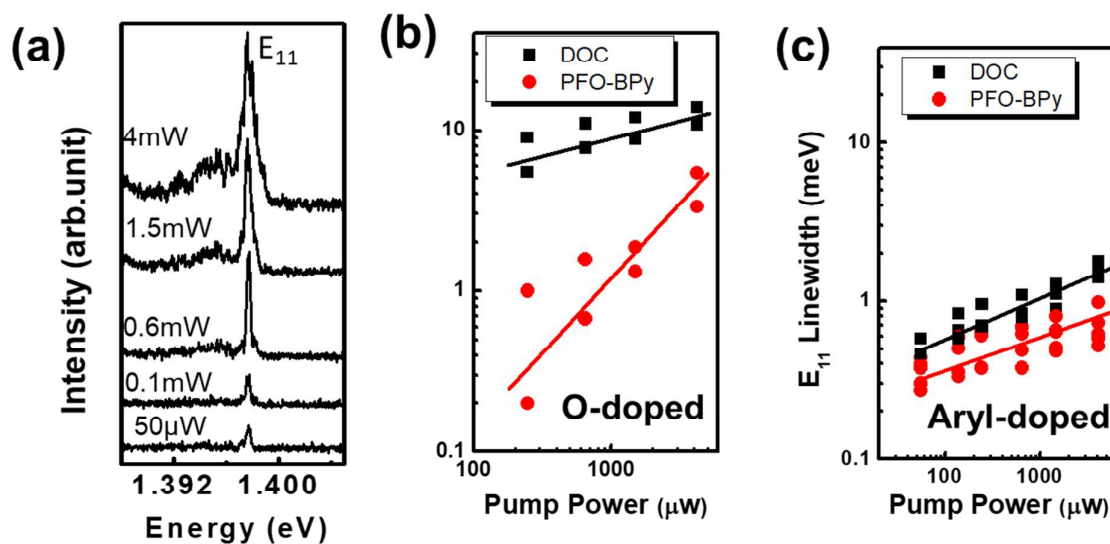


Fig. 2 Spectral linewidth study of the E_{11} exciton emission. (a) Pump power dependence of E_{11} exciton emission of LV-grown SWCNTs dispersed with PFO-Bpy. (b) E_{11} linewidths as a function of excitation power comparing DOC and PFO-BPy dispersed of LV-grown SWCNTs that are oxygen functionalized (c) E_{11} linewidths as a function of excitation power comparing DOC and PFO-BPy dispersed LV-grown SWCNTs that are functionalized with 3,5-dichlorobenzene via diazonium salts. All data are recorded at 3.8 K.

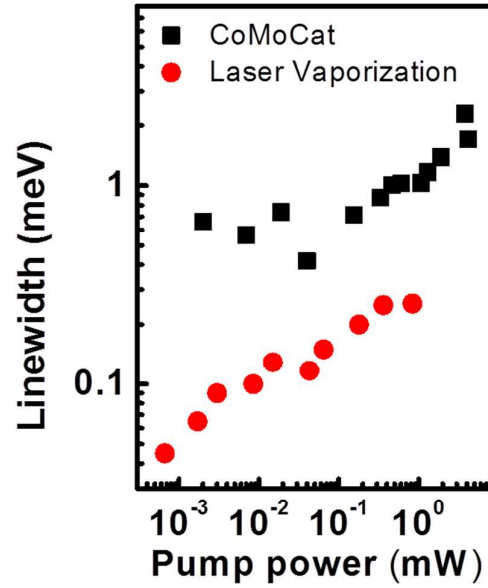


Fig. 3 Influence of growth technique on spectral linewidth. E_{11}^* linewidths as a function of excitation intensity comparing a (6,5) CoMoCat grown PFO-BPy dispersed SWCNTs as well as a (5,4) laser-vaporization-grown PFO-BPy dispersed SWCNTs. Both samples underwent the same doping procedure to create E_{11}^* . Data are recorded at 3.8 K.

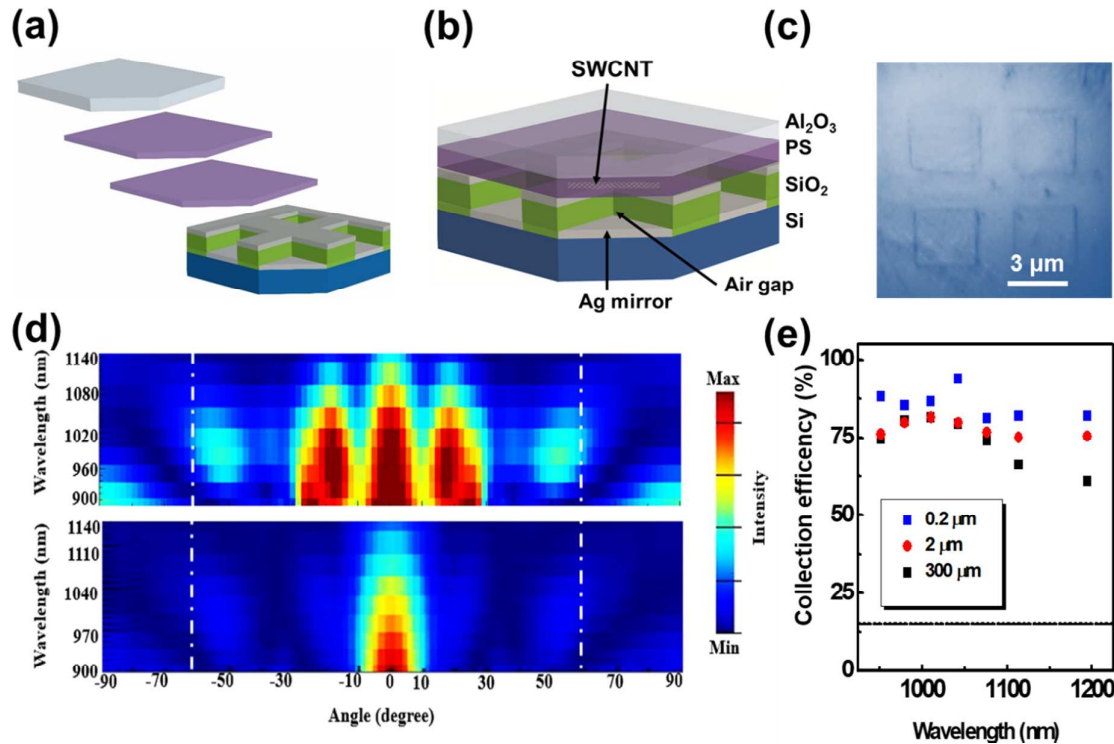


Fig. 4 Fabrication of MDA cavities with embedded SWCNTs. (a) Schematic of the realized layer sequence of the MDA cavity. Micro-patterned SiO₂ is coated with a 100 nm thick silver layer acting as a broadband mirror. Polystyrene layer (PS I) is dry stamped followed by SWCNT drop casting, stamping a PS capping layer (PS II), and finally a high index outcoupler (sapphire layer). (b) Overview of assembled MDA system. (c) Optical image of the fabricated MDA chip with embedded SWCNTs and 3 μm side lengths squares hole arrays. (d) Theoretical far-field emission profiles (emitted power density) of the MDA mode versus wavelength. Upper panel is an MDA with the actual utilized 300 μm sapphire layer and lower panel with the ideal 200 nm sapphire. Dashed line illustrates light collection cone of the objective (e) Calculated LCE for a dipole emitter positioned on bare wafer (dash line) and MDA region with different thickness of sapphire illustrating high LCE in the 1000 nm region regardless of sapphire layer thickness.

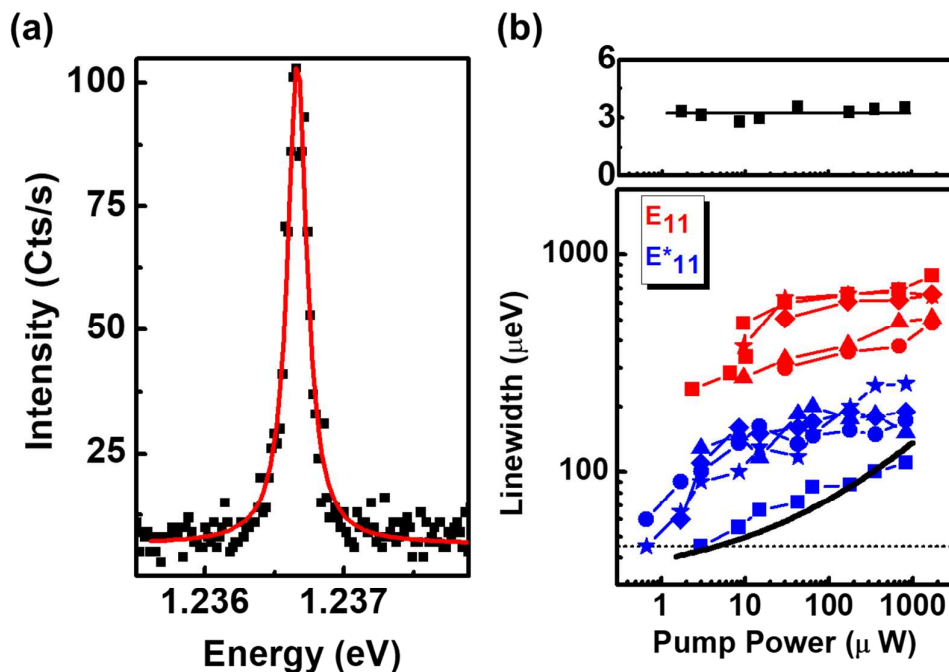
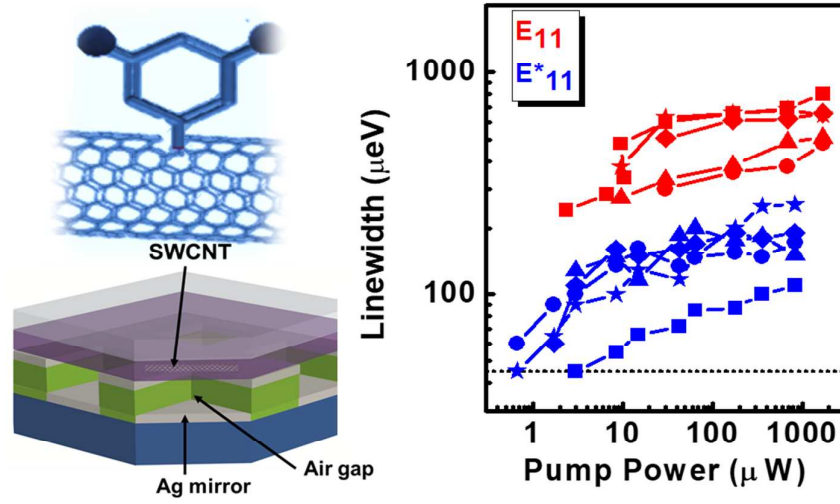


Fig. 5 Pump-power dependent spectral linewidth comparing E_{11} and E_{11}^* excitons embedded into MDA cavities. (a) High-resolution PL spectrum of the E_{11}^* exciton emission recorded for a (5,4) SWCNT (black dots). Red solid line is the corresponding Lorentzian fit function. (b) Lower panel: Pump power dependent linewidth for 3,5-dichlorobenzene-functionalized (5,4) LV-grown SWCNTs wrapped in PFO-BPy. Upper panel: Average spectral linewidth ratio between E_{11}^* and E_{11} versus pump power. The dashed lines indicate the spectral resolution limit. Lorentzian linewidth values near the spectral resolution limit were deconvolved by a Voigt function that includes additional Gaussian broadening from the spectrometer response function. The black solid-line is a fit to the charge-trap model of pump-induced exciton dephasing shown exemplarily for one case. Data are recorded at 3.8 K.



TOC Figure